Nanoparticle Size Distribution and Surface Effects on the Thermal Dependence of Magnetic Anisotropy

Guilherme Gomide,[*,†] Rafael Cabreira Gomes,[‡] Márcio Gomes Viana,[†,¶] Alex Fabiano Cortez Campos,[§] Renata Aquino,[§] Alberto López-Ortega,[‖,⊥] Régine Perzynski,[#] and Jérôme Depeyrot[†]

†*Grupo de Fluidos Complexos, Instituto de Física, Universidade de Brasília, 70919-970, Brasília, Brazil*

‡*Departamento de Física, Universidade Federal de Santa Catarina, 88040-900, Florianópolis, Brazil*

¶*Instituto Federal de Educação, Ciência e Tecnologia do Piauí, Campus Oeiras, 64500-000, Oeiras, Brasil*

§*Laboratório de Nanociência Ambiental e Aplicada, Faculdade UnB – Planaltina, Universidade de Brasília, 73345-010, Brasília, Brazil*

‖*Departamento de Ciencias, Universidad Pública de Navarra, Campus de Arrosadía, 31006 Pamplona, Spain*

⊥*Institute for Advanced Materials and Mathematics (INAMAT2), Universidad Pública de Navarra, Campus de Arrosadía, 31006, Pamplona, Spain*

#*Sorbonne Université, CNRS, PHysico-chimie des Electrolytes et Nanosyst´emes InterfaciauX, F-75005, Paris, France*

E-mail: guilhermegomide@gmail.com

Abstract

Standard approaches to investigate the anisotropy of nanoparticle assemblies are by means of either zero-field-cooled - field-cooled DC magnetization curves or by analyzing the coercivity at low temperatures. However, these methodologies are restricted to average values of anisotropy constant, without probing its temperature dependence or symmetry. In this context, analyzing the thermal dependence of coercivity arises as a more comprehensive approach to assess anisotropic properties. Here, we investigate experimentally the thermal dependence of coercivity for cobalt ferrite nanoparticle samples synthesized by different methods, in a large range of nanoparticle diameters, resulting in samples with different internal structure, surface roughness and size distribution. Our analysis consists in accounting for the size distribution and thermal dependence of the relevant variables, allowing us to access the anisotropy constant as a function of temperature. The results indicate that the surface plays an important role in the low field determined anisotropy constants, with the thermal dependence pointing to a combination of types/sources of anisotropy affecting the coercivity. While the cubic magnetocrystalline anisotropy dominates for nanoparticles with higher diameter, the influence of surface contribution increases substantially for smaller sizes. The state of the surface is shown to be key for determining the main source of anisotropy.

Introduction

The thriving recent development in the field of magnetic nanoparticles (NPs) science is in a large part due to their successful using for high-performance technological applications, for example in information storage,[1] rare-earth free permanent magnets[2,3] or as heating agents in magnetohyperthermia[4–7] and magnetic induction catalysis.[8–10] The main characteristic that defines the high versatility of magnetic NPs is their capability to become single magnetic domains, in contrast to the multi-domain regime of 2D and bulk structures. Specifically, single-domain magnetic nanoparticles have two main key features: i) a single giant

magnetic moment, presenting large fluctuations above the well-known superparamagnetic (SPM) transition, while being blocked at low temperatures and ii) the coercive field (H_c), which is expected to reach its maximum when entering the single domain size, where domain wall reversal processes are no longer available.

Indeed, the regime at which a particular NP becomes SPM is defined by its volume and density of anisotropy energy (i.e. anisotropy constant K). Magnetic anisotropy, which is usually quantified by this anisotropy constant K (anisotropy energy per volume unit), has its origin on the spin-orbit coupling with a symmetry due to the crystal structure of the material. As the size of the particles is reduced surface effects become dominant and surface spins play a major role[11–15] on the magnetic properties creating and extra anisotropy component in small NPs.[16]

Two main methodologies are well spread out in literature to calculate K: by means of zero field cooled-field cooled DC magnetization curves[17] and using the coercive field at low temperatures.[2,18] However, even if both methodologies can estimate accurately the value of the magnetic anisotropy the results obtained are confined to K values independent of the temperature and fail to determine the nature of the anisotropy symmetry. Indeed, considering that determining both parameters is fundamental to envisage novel application based on magnetic NPs, it is mandatory to develop a methodology that will help us to estimate at the same time the thermal dependence and symmetry nature of the magnetic anisotropy.

Previous works in the field[19–22] have defined the density of anisotropy energy $K(T)$, up to $\sim$65% of the Curie temperature of the material[23] in function of the saturation magnetization (M_s) as

$$\frac{K(T)}{K(0)} = \left(\frac{M_s(T)}{M_s(0)}\right)^n. \tag{1}$$

The thermal dependence of the saturation magnetization M_s follows the well-known Bloch T^α law for magnetic materials.[24–26] The exponent n arises from an expansion of the

magnetization direction in terms of the spherical harmonics. The value of this exponent varies according to the nature and symmetry of the anisotropy energy, being $n = 3$ for a uniaxial volume anisotropy, $n = 10$ for a cubic one,[16] while an exponent $n = 2$ is expected when arising from shape/surface.[27] Thus, the interfacial particularities of a given nanoparticulate system will change how its anisotropy varies with temperature, effect which is quantified by the parameter n.

We, thus, propose a systematic experimental approach by analyzing the magnetic behavior of two sets of cobalt-doped ferrite-based NPs obtained by different routes of synthesis and with average diameters ranging from 3 to 11 nm. The chosen routes to synthesize the NPs were hydrothermal coprecipitation and thermal decomposition of metalorganic precursors, techniques well known for producing nanoparticles with constrasting interfacial characteristics. While, thermal decomposition tends to produce NPs with narrow size distributions and very well-defined interfaces, NPs produced using a soft chemistry method such as hydrothermal coprecipitation lean towards a broader size distribution and higher degree of surface roughness.

We utilize the thermal dependence of coercivity to obtain deeper insight on the different sources of anisotropy in these magnetic NP assemblies. The experimental data is analyzed within the framework of Kneller's law,[28] while also taking into account the effect of size distribution and thermal dependence of both saturation magnetization and anisotropy on the coercivity.

The chosen set of samples, along with the thorough comparative analysis enables us to determine the thermal dependence of their magnetic anisotropy, as well as their symmetry, extracting, then, the exponent n, and thus, to shed light on the characteristics of the anisotropies at play.

Sample Details and Experimental Section

The first set of samples (Co#) consists in core@shell $CoFe_2O_4$@γFe_2O_3 NPs synthesized by hydrothermal coprecipitation in alkaline medium. NP's diameter is tuned by changing the synthesis pH and nature of the utilized base. A subsequent surface treatment[29] allows us to disperse them in acidic medium by creating a protective maghemite shell onto the cobalt ferrite core. The crystal lattice that configures the nanoparticle structure is formed during the coprecipitation step. Then, the shell is hydrothermally formed through two-way diffusion of cations which has been shown to contribute to surface roughness.[30] The formation of such Fe-enriched surface layer has been evidenced by morphochemical analysis using high resolution electron microscopy.[6,31] For these samples based on core@shell NPs, the maghemite volume fraction $\phi_{s/p}$ is obtained using atomic absorption spectroscopy, with the obtained concentrations of cobalt and iron being employed in a well-established chemical core@shell model.[29] An increasing proportion with decreasing diameter is obtained, as expected. Data are collected in Table 1, where the evaluated maghemite thickness $t_{sh} = \frac{d\phi_{s/p}}{6}$ and core diameter are also given.

By controlling the pH and ionic strength of the carrier liquid, we obtain magnetic colloids (ferrofluids) with long term stability and tunable NP volume fraction. For individually dispersed nanoparticles, at low concentrations (NP volume fraction $< 1\%$), the role of dipolar interactions in the dispersion is smaller than in a powder. A typical colloidal analysis, using Small Angle X-Ray Scattering experiments is presented in figure S3, and shows the typical behavior for non-interactive colloids. The data is analyzed using well-established protocols[31,32] further described in the Supporting Information along with experimental details.

To assess the effect of the dipolar interactions on the thermal dependence of coercivity, we also investigate sample Co6 in powder form, since reducing interparticle distance is a common technique to increase dipolar interactions.[33] These interactions in powders are standardly quantified by the dipolar interaction parameter $\lambda_{dd} = \frac{\mu_0 M_S^2 V}{4\pi k_B T}$, where V is the NP's volume. λ_{dd} is given in Table 1 for the powder samples at 5K. In the frozen ferrofluid dispersions,

the dipolar interactions are quantified by the parameter λ_{dd} times the NP volume fraction. It remains here always smaller than 10^{-2}. The dipolar interactions are thus negligible in the present dispersions.

Contrastingly, thermal decomposition is known for yielding NPs with lower surface roughness, which might change the role played by surface anisotropy in these nanosystems.

Then, the second set of samples (TD#) consists in narrowly distributed $Co_xFe_{3-x}O_4$ NPs, synthesized by thermal decomposition of metal-organic precursors, and is only investigated in powder form. It is worth mentioning that this second set of samples has been thoroughly investigated in a previous work,[2] where all synthesis parameters and strategies for size control are described.

Transmission Electron Microscopy is used to characterize the morphostructural properties of both sets of NPs. Note that TEM is unable to probe the true state of NP's dispersion of a ferrofluid. The TEM micrographs are presented in the top panels of Figure 1. The first row corresponds to the images for Co# samples, while the second row depicts their high resolution (HR) images. The third row collects the images for TD# series and shows the more defined NPs synthesized by thermal decomposition as compared to the coprecipitated ones.

Panels A and B of Figure 1 show the size distribution histograms of Co# and TD# series, respectively. The dashed lines correspond to the fits using the log-normal distribution, defined as

$$P(d) = \frac{1}{\sigma d\sqrt{2\pi}} \exp\Big(- \frac{ln^2(d/d_0)}{2\sigma^2}\Big), \tag{2}$$

d being the diameter, σ the polydispersity index and d_0 the median diameter of the distribution, all determined by Transmission Electron Microscopy (TEM). Table 1 collects the parameters obtained from the fits of the log-normal distribution to the histograms.

We carry out magnetometry experiments in dilute dispersions and powder to observe their magnetic behavior. The dispersions are cooled through the freezing temperature of water in zero field, so that a random distribution of the anisotropy axes is ensured. The same is

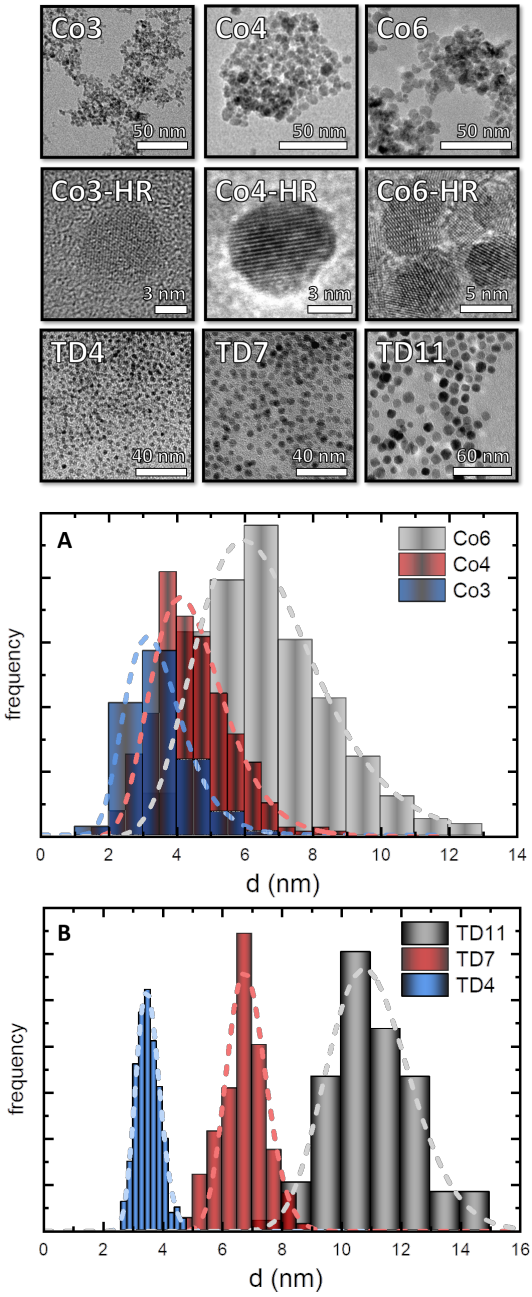

Figure 1: Top Panels: Transmission Electron Microscopy images of the studied samples. Samples are specified in each of the panels. Panel A shows the size distribution histogram of the Co# series of samples, while panel B depicts those from the TD# series. In both cases, the dashed lines indicate the best fit with the log-normal distribution.

Table 1: Basic characterization of investigated samples. d_0^{TEM} and σ^{TEM} are the median diameter and polydispersity index of the lognormal distribution of NP's diameters as determined by TEM, d_{XR} is the diameter obtained by X-ray diffraction in powder using Scherrer equation (data not shown) and M_S is saturation magnetization (measured at irreversibility field) extrapolated to zero temperature. $\phi_{s/p}$ is the volume fraction of maghemite shell for Co# samples as obtained from atomic absortion spectroscopy (AAS) measurements, leading to the shell thickness t_{sh} and to the core diameter d_{core}, using d_0^{TEM}. Samples Co3, Co4 and Co6 are prepared by hydrothermal coprecipitation in alkaline media. Samples TD4, TD7 and TD11 are prepared by thermal decomposition of metalorganic precursors. Dipolar interaction parameter λ_{dd} is given at 5K for the powder samples using the NP's diameter d_0^{TEM}. In the ferrofluid dispersions, λ_{dd} is here always smaller than unity. *For sample Co6 in powder form, the value of λ_{dd} is 50.

Sample	d_0^{TEM} (nm)	σ^{TEM}	d_{XR} (nm)	$M_S(0)$ (kA/m)	$\phi_{s/p}$ %	t_{sh} (nm)	d_{core} (nm)	λ_{dd}
Co3	3.3	0.3	3.2 (3)	220	78	0.7	12.0	0.03
Co4	4.3	0.25	4.7 (4)	329	58	0.5	3.2	0.2
Co6	6.4	0.3	7.2 (4)	321	29	0.3	5.7	0.5*
TD4	3.5	0.12	4.0 (2)	303	-	-	3.5	3
TD7	6.8	0.10	8.8 (4)	405	-	-	6.8	40
TD11	10.9	0.13	16.0 (8)	412	-	-	10.9	170

valid for the powders, which are prepared in absence of applied field. All measurements are carried out with a Quantum Design PPMS Evercool equipped with a superconducting coil with a maximum field $\mu_0 H$ of 9 T, using the vibrating sample magnetometer (VSM) option.

Hysteresis loops are recorded for all samples at different temperatures, ranging from 2 K to 400 K, depending of the nature of the samples. To better link the magnetization to the anisotropic features investigated, we consider here that, once irreversibility is achieved, the sample can be considered as "magnetically saturated", with all effective energy barrier overcame, as proposed by Gomes *et al.*[15] Also, measurements of magnetization as a function of temperature are performed at low field using the ZFC-FC protocol, for the ferrofluid samples, the highest temperature applied is 270 K, in order not to go above the freezing temperature of water, which would unlock the mechanical rotation of particles and change the relaxation properties of the system.

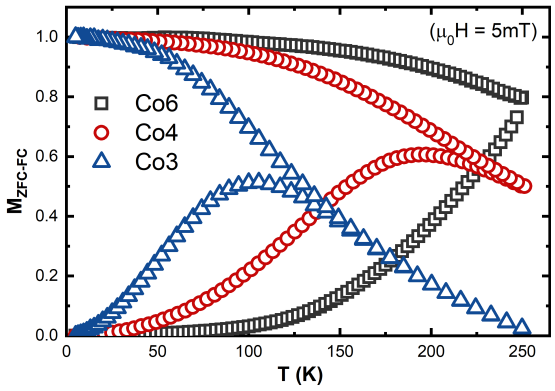

Figure 2: Temperature dependence of normalized magnetization of the samples Co3, Co4 and Co6 ferrofluids using the ZFC-FC protocol.

Experimental Results

The magnetic anisotropy of a NP assembly is commonly assessed by its blocking temperature, determined from zero-field cooled and field cooled (ZFC-FC) magnetometry experiments,[17] which gives access to the magnetic anisotropy energy. Some approaches also carry out adjustments of the ZFC-FC curves simultaneously with other curves, such as room temperature magnetization.[34] Figure 2 depicts the ZFC-FC magnetization for the Co# samples, showing an increase of the peak temperature with increasing size, but the transition to SPM state is not achieved for one of the samples (Co6), with ZFC magnetization merely approaching its peak at the maximum temperature. Thus, the measured FC curve is not a true FC curve and cannot be analyzed with any physical meaning.[35]

We, then, argue that in the case of our samples, which consist in highly anisotropic nanosized systems, the thermal dependence of coercivity is a more adapted technique for investigating the magnetic anisotropy.

Thus, we present, in the following, our results on the thermal dependence of the anisotropic features of our samples, extracted from hysteresis loops measured at various temperatures. The hysteresis loops recorded for Co3, Co4 and Co6 in dilute dispersion at 2 K are depicted in Figure 3a), and the extracted coercivity is depicted as a function of temperature in Figure 3b).

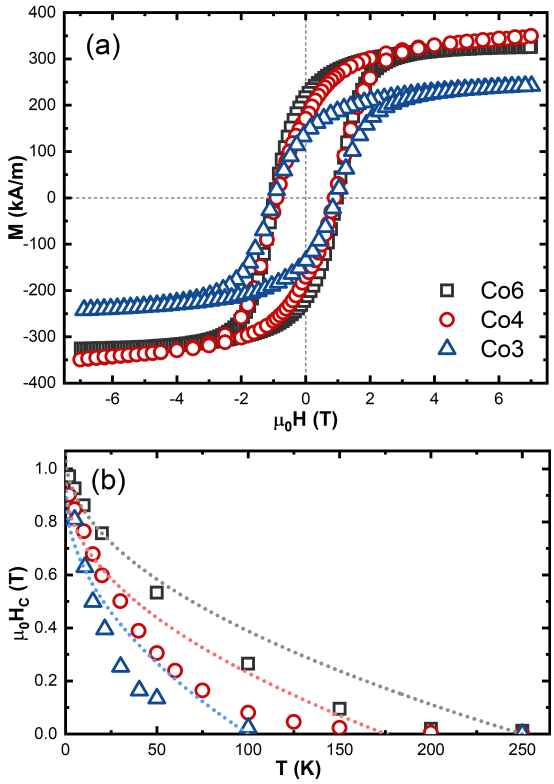

Figure 3: (a) Hysteresis loops for samples Co3 (blue triangles), Co4 (red circles) and Co6 (gray squares) measured at 2 K, in diluted dispersion. The inset closes up on the high magnetic field area, evidencing the difference of the slope in the samples. Values of magnetization are normalized by the volume fraction of particles in the ferrofluids. (b) Thermal dependence of coercivity of the same samples. The dotted lines represent the best fit of the whole data range using Kneller's law with the sample's approximate blocking temperature.

When investigating the coercive field of NP assemblies at finite temperatures, one must consider the effect of thermal agitation on the magnetic response to applied field. When descending from complete magnetic saturation, the presence of the external field reduces the height of the energy barrier allowing a thermally assisted hopping of the magnetic moment from the local energy minimum to the global one. For the sake of simplicity, we reduce here the energy landscape to only one energy barrier. The contributions given by Kneller and Luborski[28] to this matter gave rise to the so-called Kneller's law for the thermal dependence of coercivity:

$$H_c(T) = 0.48\frac{2K}{M_s}\left[1 - \left(\frac{T}{T_B}\right)^{\frac{1}{2}}\right], \tag{3}$$

where the factor 0.48 denotes randomly distributed easy axes with uniaxial anisotropy, corresponding to the coercivity defined by Stoner and Wohlfarth (SW) model,[36] and T_B the blocking temperature.

Kneller's law frequently agrees very well with experimental data at low temperatures, but often fails to explain the thermal dependence of coercivity throughout the entire range where coercive field is detectable.[37–40] We also observe that for our samples, as depicted in Figure 3(b). The lack of agreement between the experimental data and the fit is clear and points out to the necessity of finding a more appropriate model.

There are two main approaches to considering this problem. The first one consists in introducing Néel relaxation to a SW-like energy landscape, enabling the calculation of the entire hysteresis loop. Using this method, Franco and Conde calculated[41] the thermal dependence of hysteresis loops for a monodisperse sample. Another article describes a similar methodology for polydisperse assemblies with different anisotropy symmetries.[42] More recently, Richy *et al*[43] utilized this approach to simulate the temperature dependence of magnetization curves for size-distributed NP assemblies with uniaxial, biaxial[44] and also including unidirectional anisotropy constants providing insightful information regarding exchange-coupling mechanisms.

The second approach is more straightforward as far as computation goes, and it relies

on the expression obtained by Kneller, which is then weighted by the size distribution and combined with the behavior of the superparamagnetic fraction. This approach was introduced by Nunes *et al*, who investigated the effect of size distribution on the coercivity[40] by considering, at each temperature, the effect of the SPM nanoparticles. Other authors[45] considered the thermal dependency of the magnetic anisotropy, modifying the overall behaviour of Kneller's law. Our work adds to this approach by combining the thermal dependence of K and M_s while also taking into account the size distribution which dictates the thermal transition to SPM state.

This second approach, in spite of not being able to describe the NP system as thoroughly as the first one, allows us anyway to extract important insight on several experimental findings. In our case, the introduction of a thermally-dependent density if anisotropy energy K allows us to understand the evolution of coercivity as a function of temperature and gives us some clues about the NP's anisotropy symmetry through the n parameter. This thermal dependence of K can be of great value when one designs nanomaterials for application purposes, in particular for several bio-applications.

Model

Firstly, our model considers the temperature-dependent ratio between the SPM and blocked populations of a polydisperse system. Then, we explore the effects of taking into account also the thermal dependence of both magnetization and anisotropy constant.

The transition temperature between the blocked and the SPM states is volume-dependent. The critical diameter $d_c(T)$ below which NPs with uniaxial anisotropy will be in the SPM state at a given temperature can be written as

$$d_c(T) = \sqrt[3]{\frac{150 k_B T}{\pi K}}. \tag{4}$$

It illustrates that, in a polydisperse system, the ratio between the SPM and blocked

populations is temperature-dependent. This temperature dependence is directly responsible for changes in the average coercivity of a NP assembly, which go beyond the considerations of Kneller and Luborski in their original paper on this matter.

When considering a polydisperse NP assembly, equation 4 translates the fact that when thermal agitation is present, if a fraction of the NP population has $d < d_c$, it will be in the SPM regime, whilst the ones with $d > d_c$ will be blocked. One must then, follow a similar approach as the one proposed by Kneller and Luborski for binary mixtures. The key difference is that in the case of polydisperse systems, the portions of the sample in the SPM and in the blocked state change with temperature, the diameter that divides the two populations being given by the expression above. Transposing that into the actual behavior of coercivity requires understanding how exactly does an additive SPM contribution to the magnetization affects the magnetic response of the sample as a whole.

Another feature induced by the presence of size-distributed nanoparticles is a change in the overall anisotropy symmetry, which can be probed by analyzing the low temperature squareness (see Table 2). To simplify and allow a better comparison between the various samples, we consider in the calculations that the samples can be described with a single barrier of anisotropy energy (thus with effective uniaxial anisotropy symmetry and anisotropy constant K), but with a thermal dependence driven by the n parameter which indicates the actual symmetry of the NP system.

In the SPM regime, the low field magnetization increases linearly with the applied field, the proportionality constant being the superparamagnetic susceptibility. For a sample with randomly distributed anisotropy axes of the NPs, it is given by $\chi_{SPM} = \frac{\mu_0 M_s^2 V}{3k_B T}$. We can, thus, calculate the total contribution from the SPM particles at a given temperature by weighting χ_{SPM} with the size distribution $P(d)$ up to the critical diameter.

For the NPs with diameter above $d_c(T)$, we assume a Kneller-like contribution with coercivity H_{cb} (coercivity of the blocked NPs), but considering the average blocking temperature

only of the NPs in the blocked state

$$\left\langle T_B \right\rangle_T = \frac{\pi K}{150 k_B} \frac{\int_{d_c(T)}^{\infty} d^3 P(d)\, dd}{\int_{d_c(T)}^{\infty} P(d)\, dd}. \tag{5}$$

For these blocked nanoparticles, we follow Nunes *et al*[40] and assume that the magnetization varies almost linearly between the remanent magnetization M_r and the coercive field H_{cb}. This simplifies the calculations and was shown to allow an adequate determination of the coercivity. By writing the magnetization as a sum of the SPM contribution and the linear contribution of the blocked ones and solving for $M = 0$, we obtain the expression for the coercive field of the polydisperse sample at any given temperature $\left\langle H_c \right\rangle_T$. Here, it is important to evidence that, in order to enable the extraction of the anisotropy constant, we calculate the distribution of blocking temperatures instead of obtaining it experimentally from ZFC/FC curves. When determined experimentally, the distribution would carry implicitly the temperature dependence of anisotropy which would be, then, not directly accessible. In our case, it comes as a result of the fitting procedure, helping to shed light in the anisotropy mechanisms.

We also take into account the reduction of magnetization and anisotropy constant with increasing temperature, both of which induce changes in the behaviour of $\left\langle H_c \right\rangle_T$, which can be inferred by analyzing Equations 4 and 5. A more in-depth discussion can be found in the SI.

Discussion

The thermal variations of K and M_s and their effect on coercivity can only be understood by considering both quantities simultaneously. The different behaviors for $d_c(T)$, critical diameter above which NPs are in SPM state, shown in Figure S3, are clear indicators of the impact of such thermal dependences. It can be promptly inferred that a considerable fraction of the particles must be accounted as SPM instead of blocked, if the thermal dependences

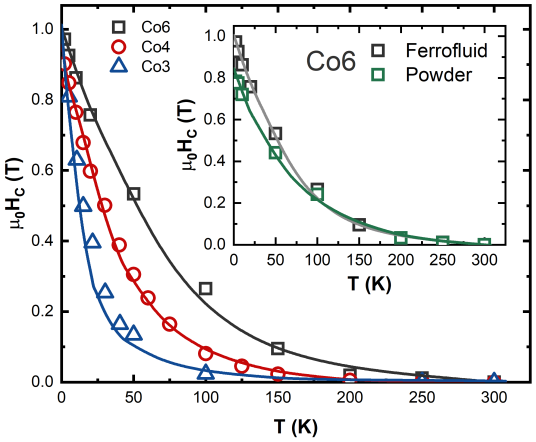

Figure 4: Experimental values of coercivity for samples Co3 (blue triangles), Co4 (red circles) and Co6 (gray squares) as a function of temperature along with the best fits using the proposed model (solid lines). Inset: Comparison between dilute ferrofluid (gray squares) and powder (green squares) for sample Co6 along with the best fits using the proposed model.

of K and M_s are taken into account. As an example, in the case of $n = 3$ in Eq. 1 (uniaxial volume anisotropy), ignoring the thermal dependence of K creates a misdetermination of d_c by approximately 50% at 270 K. That, by itself, illustrates the relevance of accounting for these thermal changes. Furthering, one can inspect the coercivity of the blocked nanoparticles H_{cb}, as shown in Figure S3(b). The increase in d_c creates a substantial reduction of H_{cb}, with considerable impact for temperatures above 25 K, in the example chosen in the figure.

We have, thus, adjusted the experimental coercivity data for the investigated samples. Figure 4 shows the experimentally determined coercivity for samples Co3, Co4 and Co6 along with their best fit using the model in its complete form. All three samples have similar coercivity at 2 K, however, when temperature starts increasing, they promptly differentiate their behavior. That, of course, is related to the earlier start of SPM transition in the samples with smallest NPs, which translates into a reduction of H_c at temperatures lower than what is observed for sample Co6 (larger NPs). The fits adjust the experimental data very well and the fitting parameters are summarized in Table 2.

The obtained parameters provide information regarding the magnetic anisotropy in the investigated samples. The values obtained for the anisotropy constant at zero temperature

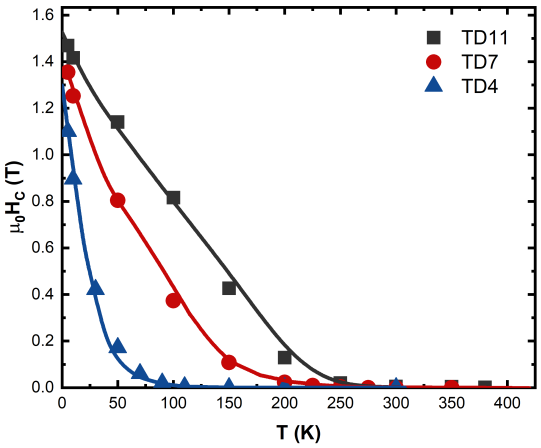

Figure 5: Experimental values of coercivity for samples TD4 (blue triangles), TD7 (red circles) and TD11 (gray squares) as a function of temperature along with the best fits using the proposed model (solid lines).

K_0 are in agreement with values in the literature, found to be between 1×10^5 and 3×10^6 J/m^3 for cobalt ferrite NPs.[33,46,47]

The different exponents point to the different nature of the anisotropy ruling the magnetization processes in each sample, as found by the model. The fact that using n = 2 improves the fit for Co3 sample indicates a more significant presence of (uniaxial) shape/surface anisotropy in this sample, which is in conformity with its very small average size and its core@shell structure. This reduction in the exponent for the smallest co-precipitated nanoparticles, together with the more pronounced diameter difference between the fit and size distribution histogram, point out to the origin of this diameter difference. In fact, a surface contribution to the magnetic anisotropy is the most likely possibility.[48]

The diameters found for Co3, Co4 and Co6 are larger than the values obtained in transmission electron microscopy. Although each technique typically has its bias as far as diameter determination goes (see inset of Fig. S3), this increase in diameter is significant and might be related to the existence of some extra contribution to magnetic anisotropy.[49,50] This hypothesis will be discussed in more detail further ahead, when we compare the results between Co and TD series.

To assess the influence of dipolar interactions, which become more important at low

Table 2: Fitting parameters used to adjust the experimental coercivity data of samples with the proposed model. d_0^{FIT} and σ^{FIT} are the median diameter and the polydispersity index of the log-normal distribution of diameters obtained by the fits with our model, K_0 the anisotropy constant at 0 K and n the power used in the $K(T)$ model. M_r/M_s is the low temperature squareness obtained experimentally at 2 K for Co# series and 5 K for TD# series.

Sample	d_0^{FIT} (nm)	σ^{FIT}	K_0 (J/m^3)	n	M_r/M_s
Co3 (Fluid)	5.8	0.33	$2.30{\cdot}10^5$	2	0.52
Co4 (Fluid)	7.2	0.33	$3.05{\cdot}10^5$	3	0.51
Co6 (Fluid)	8.1	0.28	$3.40{\cdot}10^5$	3	0.69
Co6 (Powder)	8.2	0.30	$2.90{\cdot}10^5$	3	0.63
TD4 (Powder)	4.7	0.16	$4.30{\cdot}10^5$	2	0.50
TD7 (Powder)	6.5	0.15	$6.10{\cdot}10^5$	6	0.77
TD11 (Powder)	10.6	0.20	$6.8{\cdot}10^5$	10	0.79

temperature, we compare here the fitting parameters obtained for sample Co6 in both diluted ferrofluid and powder form. As seen in Table 2, the changes in diameter and polydispersity are not considerable, the main change being a reduction in the determined value for K_0 in the powder, in a trend that follows the slightly smaller value of coercivity and is likely due to the demagnetizing nature of dipolar interactions, and thus, maintaining the coherence in the determination of n among all the samples, for which dipolar interaction is either small for dispersions of Co# (λ_{dd} smaller than 1 at 2K) and rather important for all the powder samples (λ_{dd} larger than 1 at low temperatures).

Hence, we proceed to the investigation of the thermal dependence of K in the TD series, whose measurements are carried out in powder. These fits are presented in Figure 5 and the parameters collected in Table 2. It is specially worth mentioning that in TD series, the diameters obtained are generally closer to the ones determined by TEM. That fact corroborates the hypothesis that the diameter extracted from the fit actually carries some information about additional sources of magnetic anisotropy which may have a different

temperature dependence than that of magnetocrystalline anisotropy. There are different types of magnetic anisotropy that may influence the dynamic of the NPs core magnetic moment. Since the difference in diameter is greater for the smaller samples of Co series, we can intuit that such contribution arises from surface spins which create additional anisotropy fields that affect the NPs core anisotropy, which can increase coercivity.[51] The construction of our model does not account for the presence of such types of anisotropy, so triangulating the exact source in the future using an approach that describes the energy landscapes combined with dynamic measurements[11] would help to shed light into this matter.

Another noteworthy feature is that, with increasing diameter, we observe a trend in the exponent from $n = 2$ (uniaxial shape/surface contribution) to $n = 10$ (cubic contribution)[1]. The shift to high values of the exponent implicate a more significant importance of the cubic anisotropy as size increases,[48] which is corroborated by the increase in the squareness values[2] of the samples from 0.5 to 0.8 (see Table 2). In this first approach, for the sake of simplicity and ease of comparison, we did not thoroughly consider all the modifications of this shift to cubic anisotropy in the calculations of the model other than on the exponent n. Although changes in the behavior of the relaxation times and static coercivity are to be expected, we can still extract valuable information from the temperature variation of K.

Figure 6 shows the anisotropy constants obtained for all studied samples as a function of temperature. It is also possible to extrapolate to higher temperature values (well below the Curie point). This is crucial for applications at room temperature or above. The profile of the anisotropy curves corroborates and illustrates the different rates of reduction of K with temperature for the different symmetries and types of anisotropy.

In the future, refining the analysis in order to consider other types of anisotropy and/or intra and interparticle couplings can be substantial improvements to NP magnetism studies. That can be associated with studies starting from the energy landscapes[43] with calculations of the hysteresis loops and even considering angular dependencies. Also, further studies with

[1]We interpret the value n = 6 for sample TD7 as a mixing of uniaxial and cubic anisotropy among the NP's population.

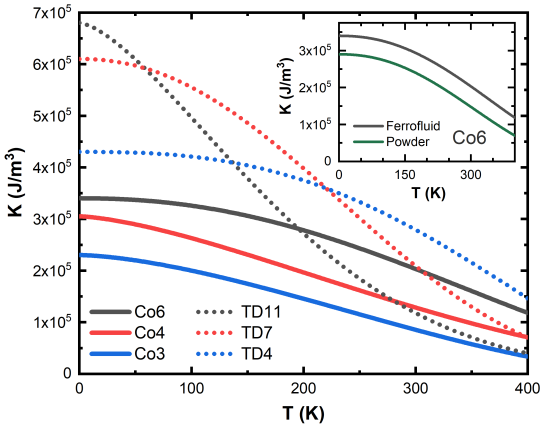

Figure 6: Anisotropy constants determined for all samples. The coprecipitation series Iin frozen dispersions) is shown in solid lines and the thermal decomposition series Iin powder) is shown in dotted lines. The inset depicts the comparison between frozen ferrofluid and powder samples of Co6.

concentrated ferrofluids and different core anisotropies should help to further enlighten the effect of dipolar interactions under controlled conditions.

Conclusions

Our study reveals that the thermal dependence of the coercive field of polydisperse nanoparticle assemblies allows one to obtain the NPs magnetic anisotropy energy per volume unit and its evolution with temperature. The model successfully describes the experimental coercivity of nanosystems based on cobalt ferrite nanoparticles elaborated by two different methods and with different average diameters.

Added to the contribution of the superparamagnetic particles and to the mean T-dependent blocking temperature, the thermal dependence of both the anisotropy constant and saturation magnetization are shown to be crucial in describing the coercivity. By using a calculated distribution of blocking temperatures, we are able to successfully determine the anisotropy constant as a function of temperature, variations usually inaccessible in these kinds of systems due to SPM relaxation.

The thermal behaviors observed for the anisotropy constants of the different samples point

out to different sources of magnetic anisotropy, which are present in different proportions depending on the size and on both crystalline and magnetic roughness of the nanoparticles interface. In the future, associating measurements with different timescales are promising in what concerns unraveling these different anisotropic contributions, helping to obtain more solid information on the magnetic behavior of nanoparticle systems.

Acknowledgement

Authors gratefully acknowledge the financial support of the Brazilian agencies CAPES, CNPq (Grants 465259/2014-6, 202340/2015-5 and 400849/2016-0), INCT-FCx (Grant 2014/50983-3) and FAP-DF (Grants 0193.001569/2017 and 0193.001376/2016). A.L.O. acknowledges support from the Universidad Pública de Navarra (Grant PJUPNA2020). The authors of University of Brasília and Sorbonne Université acknowledge support by contract CAPES/ COFECUB n○ 88881.370915/2019-01 and Ph959/20.

Supporting Information Available

In-depth discussion of the developed model, including some remarks about size distribution, and additional data: i) Hysteresis loops in different temperatures for all samples; ii) Saturation magnetization and anisotropy constant as a function of temperature for typical samples; iii) SAXS experiment showing the colloidal state of a typical sample.

References

(1) Staunton, J.; Szunyogh, L.; Buruzs, A.; Gyorffy, B.; Ostanin, S.; Udvardi, L. Temperature dependence of magnetic anisotropy: An ab initio approach. *Physical Review B* **2006**, *74*, 1–13.

(2) López-Ortega, A.; Lottini, E.; Fernández, C. d. J.; Sangregorio, C. Exploring the Magnetic Properties of Cobalt-Ferrite Nanoparticles for the Development of a Rare-Earth-Free Permanent Magnet. *Chemistry of Materials* **2015**, *27*, 4048–4056.

(3) Cui, J.; Kramer, M.; Zhou, L.; Liu, F.; Gabay, A.; Hadjipanayis, G.; Balasubramanian, B.; Sellmyer, D. Current progress and future challenges in rare-earth-free permanent magnets. *Acta Materialia* **2018**, *158*, 118–137.

(4) Garaio, E.; Sandre, O.; Collantes, J.-M.; Garcia, J. A.; Mornet, S.; Plazaola, F. Specific absorption rate dependence on temperature in magnetic field hyperthermia measured by dynamic hysteresis losses (ac magnetometry). *Nanotechnology* **2015**, *26*, 015704.

(5) Zhang, Q.; Castellanos-Rubio, I.; Munshi, R.; Orue, I.; Pelaz, B.; Gries, K. I.; Parak, W. J.; del Pino, P.; Pralle, A. Model Driven Optimization of Magnetic Anisotropy of Exchange-Coupled Core-Shell Ferrite Nanoparticles for Maximal Hysteretic Loss. *Chemistry of Materials* **2015**, *27*, 7380–7387.

(6) Pilati, V.; Cabreira Gomes, R.; Gomide, G.; Coppola, P.; Silva, F. G.; Paula, F. L. O.; Perzynski, R.; Goya, G. F.; Aquino, R.; Depeyrot, J. Core/Shell Nanoparticles of Non-Stoichiometric Zn-Mn and Zn-Co Ferrites as Thermosensitive Heat Sources for Magnetic Fluid Hyperthermia. *The Journal of Physical Chemistry C* **2018**, *122*, 3028–3038.

(7) Albino, M.; Fantechi, E.; Innocenti, C.; López-Ortega, A.; Bonanni, V.; Campo, G.; Pineider, F.; Gurioli, M.; Arosio, P.; Orlando, T. et al. Role of Zn2+ Substitution on the Magnetic, Hyperthermic, and Relaxometric Properties of Cobalt Ferrite Nanoparticles. *The Journal of Physical Chemistry C* **2019**, *123*, 6148–6157.

(8) Yassine, S. R.; Fatfat, Z.; Darwish, G. H.; Karam, P. Localized catalysis driven by the induction heating of magnetic nanoparticles. *Catalysis Science & Technology* **2020**, *10*, 3890–3896.

(9) Wang, W.; Tuci, G.; Duong-Viet, C.; Liu, Y.; Rossin, A.; Luconi, L.; Nhut, J.-M.; Nguyen-Dinh, L.; Pham-Huu, C.; Giambastiani, G. Induction Heating: An Enabling Technology for the Heat Management in Catalytic Processes. *ACS Catalysis* **2019**, *9*, 7921–7935.

(10) Varsano, F.; Bellusci, M.; La Barbera, A.; Petrecca, M.; Albino, M.; Sangregorio, C. Dry reforming of methane powered by magnetic induction. *International Journal of Hydrogen Energy* **2019**, *44*, 21037–21044.

(11) Silva, F. G.; Depeyrot, J.; Raikher, Y. L.; Stepanov, V. I.; Poperechny, I. S.; Aquino, R.; Ballon, G.; Geshev, J.; Dubois, E.; Perzynski, R. Exchange-bias and magnetic anisotropy fields in core–shell ferrite nanoparticles. *Scientific Reports* **2021**, *11*, 5474.

(12) Obaidat, I. M.; Mohite, V.; Issa, B.; Tit, N.; Haik, Y. Predicting a major role of surface spins in the magnetic properties of ferrite nanoparticles. *Crystal Research and Technology* **2009**, *44*, 489–494.

(13) Nathani, H.; Gubbala, S.; Misra, R. D. Magnetic behavior of nanocrystalline nickel ferrite: Part I. The effect of surface roughness. *Materials Science and Engineering B: Solid-State Materials for Advanced Technology* **2005**, *121*, 126–136.

(14) Berkowitz, A. E.; Kodama, R. H.; Makhloul, S. A.; Parker, F. T.; Spada, F. E.; McNiff, E. J.; Foner, S. Anomalous properties of magnetic nanoparticles. *Journal of Magnetism and Magnetic Materials* **1999**, *196*, 591–594.

(15) Gomes, R. C.; da Silva, F. G.; Muniz, T. Q.; Gomide, G.; Pilati, V.; Aquino, R.; Geshev, J.; Perzynski, R.; Depeyrot, J. Magnetic irreversibility and saturation criteria in ultrasmall bi-magnetic nanoparticles. *Journal of Alloys and Compounds* **2020**, 153646.

(16) Cullity, B. D.; Graham, C. D. *Introduction to magnetic materials*, 2nd ed.; Wiley: New Jersey, 2009.

(17) Bruvera, I. J.; Mendoza Zélis, P.; Pilar Calatayud, M.; Goya, G. F.; Sánchez, F. H. Determination of the blocking temperature of magnetic nanoparticles: The good, the bad, and the ugly. *Journal of Applied Physics* **2015**, *118*, 184304.

(18) Muscas, G.; Yaacoub, N.; Concas, G.; Sayed, F.; Hassan, R. S.; Greneche, J. M.; Cannas, C.; Musinu, A.; Foglietti, V.; Casciardi, S. et al. Evolution of the magnetic structure with chemical composition in spinel iron oxide nanoparticles. *Nanoscale* **2015**, *7*, 13576–13585.

(19) van Vleck, J. H. On the Anisotropy of Cubic Ferromagnetic Crystals. *Physical Review* **1937**, *52*, 1178–1198.

(20) Zener, C. Classical Theory of the Temperature Dependence of Magnetic Anisotropy Energy. *Physical Review* **1954**, *96*, 1335–1337.

(21) Keffer, F. Temperature Dependence of Ferromagnetic Anisotropy in Cubic Crystals. *Physical Review* **1955**, *100*, 1692–1698.

(22) Carr, W. J. Temperature Dependence of Ferromagnetic Anisotropy. *Physical Review* **1958**, *109*, 1971–1976.

(23) Callen, H. B.; Callen, E. The present status of the temperature dependence of magnetocrystalline anisotropy, and the l(l+1)2 power law. *Journal of Physics and Chemistry of Solids* **1966**, *27*, 1271–1285.

(24) Blundell, S. *Magnetism in Condensed Matter*; Oxford Master Series in Condensed Matter Physics; OUP Oxford, 2001.

(25) Vázquez-Vázquez, C.; López-Quintela, M. A.; Buján-Núñez, M. C.; Rivas, J. Finite size and surface effects on the magnetic properties of cobalt ferrite nanoparticles. *Journal of Nanoparticle Research* **2011**, *13*, 1663–1676.

(26) Aquino, R.; Depeyrot, J.; Sousa, M. H.; Tourinho, F. A.; Dubois, E.; Perzynski, R. Magnetization temperature dependence and freezing of surface spins in magnetic fluids based on ferrite nanoparticles. *Physical Review B* **2005**, *72*, 184435.

(27) He, L.; Chen, C. Effect of temperature-dependent shape anisotropy on coercivity for aligned Stoner-Wohlfarth soft ferromagnets. *Physical Review B* **2007**, *75*, 184424.

(28) Kneller, E. F.; Luborsky, F. E. Particle Size Dependence of Coercivity and Remanence of Single-Domain Particles. *Journal of Applied Physics* **1963**, *34*, 656.

(29) Gomes, J. A.; Sousa, M. H.; Tourinho, F. A.; Aquino, R.; Depeyrot, J.; Dubois, E.; Perzynski, R. Synthesis of Core-Shell Ferrite Nanoparticles for Ferrofluids: Chemical and Magnetic Analysis. *J. Phys. Chem. C* **2008**, *112*, 6220–6227.

(30) Gomes, J. A.; Azevedo, G. M.; Depeyrot, J.; Mestnik-Filho, J.; Paula, F. L.; Tourinho, F. A.; Perzynski, R. Structural, chemical, and magnetic investigations of core-shell zinc ferrite nanoparticles. *Journal of Physical Chemistry C* **2012**, *116*, 24281–24291.

(31) Pilati, V.; Gomide, G.; Gomes, R. C.; Goya, G. F.; Depeyrot, J. Colloidal Stability and Concentration Effects on Nanoparticle Heat Delivery for Magnetic Fluid Hyperthermia. *Langmuir* **2021**, *37*, 1129–1140.

(32) Mériguet, G.; Wandersman, E.; Dubois, E.; Cebers, A.; Gomes, J. A.; Demouchy, G.; Depeyrot, J.; Robert, A.; Perzynski, R. Magnetic fluids with tunable interparticle interaction: Monitoring the under-field local structure. *Magnetohydrodynamics* **2012**, *48*, 415–425.

(33) Vieira, C. A.; Gomes, R. C.; Silva, F. G.; Dias, A. L.; Aquino, R.; Campos, A. F.; Depeyrot, J. Blocking and remanence properties of weakly and highly interactive cobalt ferrite based nanoparticles. *Journal of Physics Condensed Matter* **2019**, *31*, 175801.

(34) Tamion, A.; Hillenkamp, M.; Tournus, F.; Bonet, E.; Dupuis, V. Accurate determination of the magnetic anisotropy in cluster-assembled nanostructures. *Applied Physics Letters* **2009**, *95*, 062503.

(35) Aquino, V. R. R.; Vinícius-Araújo, M.; Shrivastava, N.; Sousa, M. H.; Coaquira, J. A.; Bakuzis, A. F. Role of the Fraction of Blocked Nanoparticles on the Hyperthermia Efficiency of Mn-Based Ferrites at Clinically Relevant Conditions. *Journal of Physical Chemistry C* **2019**, *123*, 27725–27734.

(36) Stoner, E. C.; Wohlfarth, E. P. A Mechanism of Magnetic Hysteresis in Heterogeneous Alloys. *IEEE Transactions on Magnetics* **1947**, *27*, 3475–3518.

(37) Winkler, E. L.; Lima, E.; Tobia, D.; Saleta, M. E.; Troiani, H. E.; Agostinelli, E.; Fiorani, D.; Zysler, R. D. Origin of magnetic anisotropy in ZnO/CoFe 2 O 4 and CoO/CoFe 2 O 4 core/shell nanoparticle systems. *Applied Physics Letters* **2012**, *101*, 252405.

(38) Lima, E.; Winkler, E. L.; Tobia, D.; Troiani, H. E.; Zysler, R. D.; Agostinelli, E.; Fiorani, D. Bimagnetic CoO Core/CoFe 2 O 4 Shell Nanoparticles: Synthesis and Magnetic Properties. *Chemistry of Materials* **2012**, *24*, 512–516.

(39) Lavorato, G.; Lima, E.; Tobia, D.; Fiorani, D.; Troiani, H. E.; Zysler, R.; Winkler, E. L. Size effects in bimagnetic CoO/CoFe2O4 core/shell nanoparticles. *Nanotechnology* **2014**, *25*, 355704.

(40) Nunes, W. C.; Folly, W. S. D.; Sinnecker, J. P.; Novak, M. A. Temperature dependence of the coercive field in single-domain particle systems. *Physical Review B* **2004**, *70*, 014419.

(41) Franco, V.; Conde, A. Thermal effects in a Stoner-Wohlfarth model and their influence on magnetic anisotropy determination. *Journal of Magnetism and Magnetic Materials* **2004**, *278*, 28–38.

(42) Tamion, A.; Bonet, E.; Tournus, F.; Raufast, C.; Hillion, A.; Gaier, O.; Dupuis, V. Efficient hysteresis loop simulations of nanoparticle assemblies beyond the uniaxial anisotropy. *Physical Review B - Condensed Matter and Materials Physics* **2012**, *85*, 134430.

(43) Richy, J.; Jay, J.-P.; Pogossian, S. P.; Youssef, J. B.; Sheppard, C. J.; Prinsloo, A. R. E.; Spenato, D.; Dekadjevi, D. T. Thermal simulation of magnetization reversals for size-distributed assemblies of core-shell exchange biased nanoparticles. *Journal of Applied Physics* **2016**, *120*, 083905.

(44) Ryon, N.; Richy, J.; Sheppard, C. J.; Prinsloo, A. R. E.; Fessant, A.; Jay, J.-P.; Spenato, D.; Dekadjevi, D. T. Thermal simulation of magnetization reversals for a size-distributed assembly of nanoparticles with uniaxial and cubic anisotropies. *Journal of Applied Physics* **2019**, *126*, 133901.

(45) Torres, T. E.; Lima, E.; Mayoral, A.; Ibarra, A.; Marquina, C.; Ibarra, M. R.; Goya, G. F. Validity of the Néel-Arrhenius model for highly anisotropic CoxFe3-xO4 nanoparticles. *Journal of Applied Physics* **2015**, *118*, 183902.

(46) Ngo, A. T.; Bonville, P.; Pileni, M. P. Spin canting and size effects in nanoparticles of nonstoichiometric cobalt ferrite. *Journal of Applied Physics* **2001**, *89*, 3370–3376.

(47) Peddis, D.; Mansilla, M. V.; Mørup, S.; Cannas, C.; Musinu, A.; Piccaluga, G.; D'Orazio, F.; Lucari, F.; Fiorani, D. Spin-canting and magnetic anisotropy in ultrasmall CoFe2O 4 nanoparticles. *Journal of Physical Chemistry B* **2008**, *112*, 8507–8513.

(48) Chatterjee, B. K.; Ghosh, C. K.; Chattopadhyay, K. K. Temperature dependence of magnetization and anisotropy in uniaxial NiFe2O4 nanomagnets: Deviation from the Callen-Callen power law. *Journal of Applied Physics* **2014**, *116*, 153904.

(49) Vargas, J. M.; Nunes, W. C.; Socolovsky, L. M.; Knobel, M.; Zanchet, D. Effect of

dipolar interaction observed in iron-based nanoparticles. *Physical Review B - Condensed Matter and Materials Physics* **2005**, *72*, 184428.

(50) Kechrakos, D.; Trohidou, K. N. Magnetic properties of self-assembled interacting nanoparticles. *Applied Physics Letters* **2002**, *81*, 4574–4576.

(51) Geshev, J.; Pereira, L. G.; Schmidt, J. E. Rotatable anisotropy and coercivity in exchange-bias bilayers. *Physical Review B - Condensed Matter and Materials Physics* **2002**, *66*, 1–8.

TOC Graphic

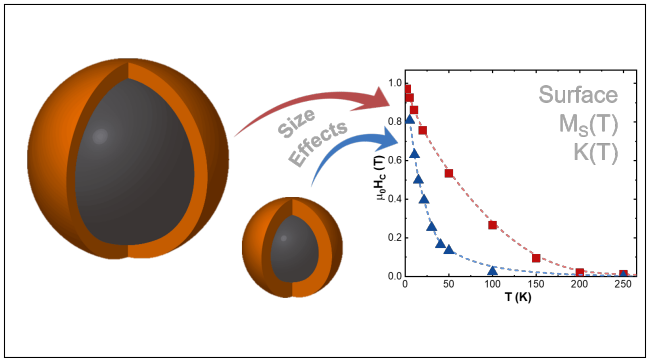
Size
Effects
Surface
$M_S(T)$
K(T)
$\mu_0 H_c$ (T)
T (K)
0.0
0.2
0.4
0.6
0.8
1.0
0
50
100
150
200
250